PCCP

PAPER

View Article Online
View Journal | View Issue

Cite this: *Phys. Chem. Chem. Phys.*, 2019, **21**, 5274

Reaction pathways for HCN on transition metal surfaces†

Mohammed Abdel-Rahman,[a] Xu Feng,[a] Mark Muir,[a] Kushal Ghale,[b] Ye Xu[b] and Michael Trenary*[a]

Received 10th December 2018,
Accepted 1st February 2019

DOI: 10.1039/c8cp07548d

rsc.li/pccp

The adsorption and decomposition of HCN on the Pd(111) and Ru(001) surfaces have been studied with reflection absorption infrared spectroscopy and density functional theory calculations. The results are compared to earlier studies of HCN adsorption on the Pt(111) and Cu(100) surfaces. In all cases the initial adsorption at low temperatures gives rise to a ν(C–H) stretch peak at ~3300 cm^{-1}, which is very close to the gas phase value indicating that the triple CN bond is retained for the adsorbed molecule. When the Pd(111) surface is heated to room temperature, the HCN is converted to the aminocarbyne species, CNH_2, which was also observed on the Pt(111) surface. DFT calculations confirm the high stability of CNH_2 on Pd(111), and suggest a bi-molecular mechanism for its formation. When HCN on Cu(100) is heated, it desorbs without reaction. In contrast, no stable intermediates are detected on Ru(001) as the surface is heated, indicating that HCN decomposes completely to atomic species.

1. Introduction

The adsorption and reactions of hydrogen cyanide on transition metal surfaces have been widely studied. These studies have been motivated in part by the relevance of the surface chemistry of molecules containing CN bonds to various areas of heterogeneous catalysis. At a more fundamental level, as a relatively small molecule that is isoelectronic with the prototypical molecular adsorbate CO, HCN offers an opportunity for a detailed mapping of its bonding structure and reaction pathways by both experimental and theoretical methods. Here we present a study that combines surface vibrational spectroscopy with density functional theory calculations of HCN interaction with the Pd(111), Ru(001) and Cu(100) surfaces. The present study was motivated in part by the marked contrast in the reported structure and reactions of HCN on Pd(111) with those on Pt(111). Kordesch *et al.* observed a vibrational loss with high resolution electron energy loss spectroscopy (HREELS) at 1540 cm^{-1} following HCN adsorption on Pd(111) at 300 K.[1,2] This frequency is characteristic of a C═N double bond from which they concluded that HCN bonds to the surface in a di-σ configuration with the C═N bond parallel to the surface. A NEXAFS study confirmed this orientation for the CN bond.[1]

In a series of papers,[3–8] we have used the technique of reflection absorption infrared spectroscopy (RAIRS) to investigate the structure and reactions of HCN on Pt(111). At a temperature of 85 K, we found that HCN adsorbs molecularly with the axis oriented perpendicularly to the surface. This was based on the strong similarity of the infrared spectrum of the absorbed molecule to that of gas phase HCN. In particular, the CH stretch of HCN on Pt(111) was observed at 3298–3000 cm^{-1}, compared to values of 3311–3312 cm^{-1} in the gas phase[9,10] and 3305–3306 cm^{-1} in an argon matrix.[11,12] As the CH stretch frequency is a sensitive indicator of the hybridization on the C atom, the observed value indicates that the adsorbed molecule retains a CN triple bond. The CN stretch is very weak for HCN on Pt(111), which is also characteristic of the gas phase and matrix-isolated molecule. For HCN adsorbed with a perpendicular orientation, the CH and CN stretches would be surface IR allowed but the bending mode would be forbidden. The latter occurs at 712 cm^{-1} in the gas phase,[9,10] which was below the low wavenumber cut-off in our RAIRS studies. However, we detected a peak at 1311 cm^{-1} that we assigned to the overtone of the bending fundamental. These spectral characteristics of HCN adsorbed at low temperature on Pt(111) led us to conclude that the molecule bonds to a Pt atom through the nitrogen lone pair in a perpendicular orientation.

When HCN is adsorbed on Pt(111) at low temperature and then warmed to 300 K, pronounced changes are observed in the RAIR spectra. The peaks associated with HCN are replaced with ones at 3363, 1567, and 1323 cm^{-1}, which were assigned to an NH_2 symmetric stretch, an NH_2 scissor mode, and a C═N stretch, respectively, of an aminocarbyne (CNH_2) species.[3] These assignments were supported by observing isotopic shifts after adsorbing

[a] *Department of Chemistry, University of Illinois at Chicago, 845 W Taylor Street, Chicago, IL 60607, USA. E-mail: mtrenary@uic.edu*
[b] *Cain Department of Chemical Engineering, Louisiana State University, Baton Rogue, LA, USA*

† Electronic supplementary information (ESI) available: Addition RAIR spectra for HCN isotopologues on Pd(111); TPRS results for HCN on Pd(111). See DOI: 10.1039/c8cp07548d

$H^{13}C^{14}N$ and $H^{12}C^{15}N$. Subsequent density functional theory calculations based on small Pt cluster models of the Pt(111) surface were used to accurately simulate the observed RAIR spectrum and isotopic shifts of aminocarbyne on Pt(111).[13] Other theoretical calculations showed that aminocarbyne is a stable species on Pt(111) and that it bonds with the CN axis perpendicular to the surface.[14,15] In independent work, aminocarbyne has also been identified as a stable intermediate on Rh(111) in the decomposition of methyl amine[16] and azomethane.[17]

The previous work arguing that HCN adsorbs on Pd(111) at 300 K with a CN double bond parallel to the surface did not consider the possibility of reaction to form a new chemical entity, such as CNH_2. The present study is designed to determine if HCN displays qualitatively different behaviour on Pt(111) and Pd(111), as suggested by past studies. By observing with RAIRS small isotopic shifts with ^{13}C and ^{15}N substitution, we show that CNH_2 does indeed form on Pd(111). Furthermore, our DFT calculations suggest that CNH_2 can form at very low temperatures and is stable to 350 K on Pd(111), just as it is on Pt(111).

On the Ru(001) surface, no RAIRS peaks are observed after annealing the surface to temperatures of 150 K or higher. From this observation, we conclude that HCN dissociates completely to atomic H, C, and N. At the other extreme of reactivity, on Cu(100), HCN was found to desorb molecularly without reaction. Based on the similarity of the low temperature and low coverage RAIR spectra for HCN on Pt(111), Pd(111), Ru(001) and Cu(100), we conclude that HCN can adsorb in a common metastable form on these surfaces that is independent of its subsequent reactive chemistry.

2. Experimental

The experiments on Pd(111) were conducted in an ultrahigh vacuum (UHV) chamber equipped for RAIRS, temperature programed reaction spectroscopy (TPRS), X-ray photoelectron spectroscopy (XPS), and low energy electron diffraction (LEED). The apparatus as well as the details of the crystal mounting and cleaning procedures are described in a recent publication.[18] The Ru(001) experiments were conducted in a separate UHV chamber equipped for RAIRS, TPRS, Auger electron spectroscopy and LEED. This apparatus and the crystal mounting and cleaning procedure are described elsewhere.[19]

Hydrogen cyanide was synthesized using the method of Hagans *et al.* in which potassium cyanide was reacted with H_2SO_4(aq).[20] Natural abundance KCN was purchased from Aldrich Chemical Company with a quoted purity of 97%. $H^{13}C^{14}N$ and $H^{12}C^{15}N$ were synthesized using the same procedure with $K^{13}C^{14}N$ and $K^{12}C^{15}N$, which were purchased from Cambridge Isotope Laboratories with quoted purities of 99 and 98+%, respectively. The purity of the HCN gases was checked with mass spectrometry and no impurities were detected.

3. Computational methods

Self-consistent, periodic DFT calculations were performed using the Vienna Ab Initio Simulations Package (VASP v5.2 and above[21]) with the optB86b van der Waals (vdW) functional developed by Klimeš *et al.*[22,23] as well as the GGA-RPBE functional[24] for comparison. Core electrons were described by the projector augmented wave (PAW) method[25,26] and the Kohn–Sham valence states (including Pd(4d5s); Ru(4d5s); N(2s2p); C(2s2p); and H(1s)) were expanded in a plane wave basis set up to a cutoff energy of 500 eV. The electronic states were smeared using a first-order Methfessel–Paxton scheme with a temperature of 0.075 eV.[27] All total energies were extrapolated back to 0 K.

The lattice constants were calculated to be 3.906 Å for Pd, 3.602 Å for Cu and 2.704/4.259 Å for Ru using the optB86b vdW functional, in close agreement with measured values (3.92 Å, 3.61 Å and 2.70/4.266 Å, respectively[28]). In comparison, the RPBE lattice constant for Pd is 3.941 Å. The fcc(111) and hcp(001) facets were each modeled using a four-layer slab with a (2×2) surface unit cell, and the Brillouin zone was sampled on a $7 \times 7 \times 1$ Monkhorst–Pack k-point mesh, respectively. A vacuum space of $\sim$16 Å was included in the z direction to minimize interactions of neighboring images, together with electrostatic decoupling in the z direction.[29] The top two layers of metal atoms were fully relaxed, with the bottom two fixed at bulk positions. Geometric optimization (*i.e.* structural relaxation) was converged to 0.01 eV $Å^{-1}$ for each relaxed degree of freedom. Energy-minimized states were verified to have no imaginary frequencies except for upright HCN in GGA-RPBE.

Adsorption energies were calculated as $\Delta E = E_{total} - E_{slab} - E_{mol}$, where E_{total}, E_{slab}, and E_{mol} are the energies of the surface with the adsorbate, the clean surface without any adsorbate, and the adsorbate molecule isolated in the gas phase in a neutral state (closed-shell or radical), respectively. A more negative ΔE therefore corresponds to stronger adsorption. The minimum-energy reaction path for an elementary step and the transition state (TS) associated with it were determined using the climbing-image nudged elastic band (CI-NEB) method[30] and the dimer method.[31] The activation energy was calculated as $E_a = E_{TS} - E_{IS}$, where IS and TS denote the initial state and transition state, respectively. Each TS was verified to possess only one vibrational mode with negative curvature in the direction of the bond being broken or formed. The transition state search was converged to 0.03 eV $Å^{-1}$ for each relaxed degree of freedom.

The simulated IR spectra of surface adsorbates were calculated using the Atomic Simulation Environment.[32] The vibrational modes and frequencies were calculated from a finite difference approximation of the dynamical matrix, and the IR intensities were calculated from a finite difference approximation of the gradient of the dipole moment in the z direction.[32] The magnitude of the displacement was 0.01 Å in each relaxed degree of freedom. The zero-point energies (ZPE) were calculated from the vibrational frequencies (ν_i) of a molecule as:

$$E^{ZPE} = \frac{1}{2}\sum_i h\nu_i$$

4. Results

4.1 RAIR spectra

The changes in the RAIR spectra for increasing exposure of HCN to Ru(001) at 90 K are shown in Fig. 1. Similar behaviour

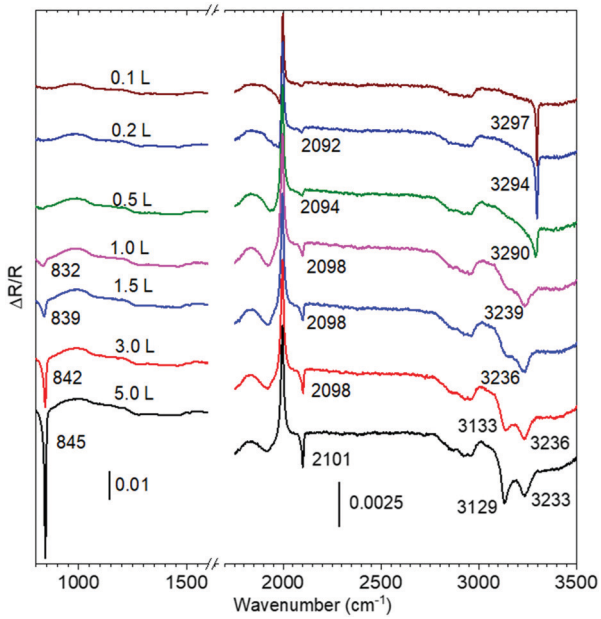

Fig. 1 RAIR spectra for increasing exposures of HCN to Ru(001) at 90 K. The positive peak just below 2000 cm^{-1} is due to adsorbed CO that is displaced and shifted upon HCN adsorption.

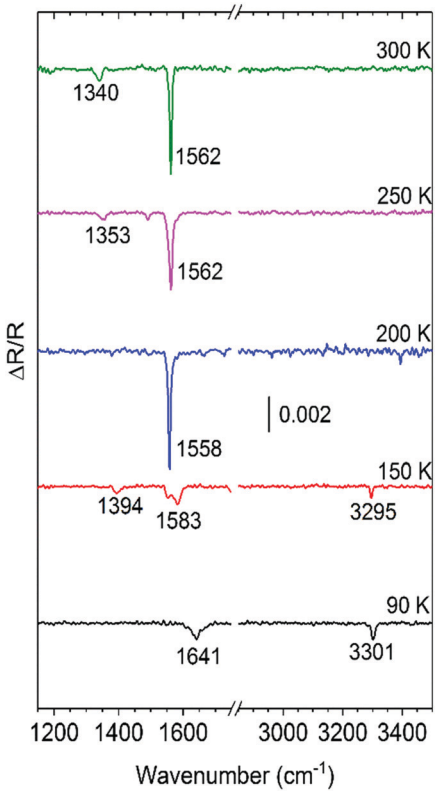

Fig. 2 RAIR spectra of $H^{12}C^{14}N$ after exposure of 1.0 L to Pd(111) and annealing to the indicated temperatures. These spectra were obtained with 4096 scans, corresponding to approximately 16 minutes per spectrum.

was observed on Pd(111) and Pt(111).[6] For the highest exposures, HCN forms a multilayer and the spectra are similar to those reported previously for solid HCN.[33–36] As a linear triatomic molecule, HCN has three fundamentals: the CH and CN stretches and the bending mode. At the lowest exposure, only the CH stretch at 3297 cm^{-1} is observed. As the exposure increases, it changes from a single-sharp peak in the 0.1 L spectrum, to a broader pair of peaks 3233 and 3129 cm^{-1} after a 5 L exposure. In the solid, HCN forms linear chains of hydrogen-bonded molecules and the strong red-shift and broadening of the CH stretch is consistent with the formation of hydrogen bonds in the multilayer. For the multilayer, the bending fundamental at 845 cm^{-1} is by far the most intense. The CN stretch, seen at 2101 cm^{-1} in the 5.0 L spectrum, is notably weak relative to the other fundamentals for gas and solid phase HCN and for HCN in an Ar matrix and is thus an intrinsic characteristic of the molecule. The CH stretch at 3297 cm^{-1} is close to the value of gas phase HCN[9] at 3312 and of HCN in an Ar matrix[11,12] at 3305–3306 cm^{-1}. As this value is indicative of the hybridization of the carbon atom, it follows that the adsorbed HCN retains a CN triple bond. The spectra at low coverages are thus most consistent with an HCN molecule bonded through the nitrogen lone pair with the axis perpendicular to the surface. With this orientation, the bending mode would not be surface IR allowed. However, the overtone of the bend would be allowed, and peaks assigned to it were observed at 1311–1323 cm^{-1} on Pt(111)[3,6] and at 1395 on Cu(100).[6] No peak clearly attributable to the bending overtone is observed for low coverages on Ru(001), although there are broad but weak features in this spectral region.

Upon annealing the HCN covered Ru(001) surface to 150 K and above, all peaks disappear from the RAIR spectrum. We interpret this as indicating complete dissociation to atomic species. A distinctly different change is seen in the RAIR spectra of HCN on Pd(111), as shown in Fig. 2. After exposing the Pd(111) surface at 90 K to 1.0 L of $H^{12}C^{14}N$, two peaks are seen at 1641 and 3301 cm^{-1}. These are assigned to molecularly adsorbed HCN. As for HCN on Ru(001), the value of the CH stretch is indicative of an sp-hybridized carbon atom, thus implying a triple CN bond.

The assignment of the peak at 1641 cm^{-1} is less straightforward. In solid HCN,[33–35] the overtone of the bending mode occurs at 1621–1632 cm^{-1} whereas it is at 1427 cm^{-1} in an Ar matrix[12] and at 1412 cm^{-1} in gas phase HCN.[37] For HCN on Pt(111) and Cu(100), we assigned peaks at 1311 and 1395 cm^{-1} to the bending overtone.[3,6] The peak observed at 1641 cm^{-1} in Fig. 2 could be plausibly assigned to the bending overtone, but this frequency is also consistent with a CN double bond stretch. One way to distinguish between these two possibilities is through isotopic shifts. Table 1 compares the values of the HCN bending modes and CN stretch modes of gas phase HCN and of CNH_2 on Pt(111) upon substitution with ^{13}C and ^{15}N along with the ratio of the shifted frequencies. As the values of the bending overtone for the ^{13}C and ^{15}N isotopologues of HCN in an Ar matrix are not available in the literature, the frequencies given in Table 1 are simply twice the fundamentals given by Nakagawa and Morino.[10] With ratios of 0.9872 and 0.9884 upon ^{13}C and ^{15}N substitution, the peak on Pd(111) shows shifts similar to those seen on Pt(111) for the peak assigned to the bending

Table 1 Wavenumber (cm^{-1}) positions of infrared peaks of HCN isotopologues and ratios (in parentheses) of positions relative to $H^{12}C^{14}N$

	$H^{12}C^{14}N$	$H^{13}C^{14}N$	$H^{12}C^{15}N$
δ(HCN), Ar matrix[11]	721	715 (0.9917)	720 (0.9986)
2× δ(HCN), Ar matrix[11]	1442	1430 (0.9917)	1440 (0.9986)
ν(CN), gas[10]	2097	2063 (0.9838)	2064 (0.9838)
2× δ(HCN), Pt(111)[3]	1311	1295 (0.9878)	1303 (0.9939)
2× δ(HCN), Pd(111)	1641	1620 (0.9872)	1622 (0.9884)
ν(CN), CNH_2 Pt(111)[3]	1323	1290 (0.9751)	1312 (0.9917)

mode overtone, despite the rather different frequencies (1641 *vs.* 1311 cm^{-1}). Moreover, these shifts are notably different from what is seen for the CN bond stretch of gas phase HCN or of CNH_2 on Pt(111), where the bond-order is between one and two. We therefore assign the 1641 cm^{-1} peak for HCN adsorbed at low temperature on Pd(111) to the overtone of the bending mode. This mode would be surface IR allowed for an upright HCN orientation, although the bending fundamental would not be allowed. While a wavenumber value of 1641 cm^{-1} is consistent with a C═N stretch, a C═N double bond implying sp^2 hybridization on the carbon atom is not consistent with the high value of the CH stretch peak at 3301 cm^{-1}.

The RAIR spectra in Fig. 2 show that as the HCN covered Pd(111) surface is heated, the peaks associated with adsorbed HCN are replaced by a new set of peaks, the most prominent of which is at 1562 cm^{-1} in the 250 and 300 K spectra. In the 150 K spectrum the reaction is incomplete with some adsorbed HCN still present as indicated by the CH stretch at 3295 cm^{-1}. The spectra in Fig. 2 were obtained with 4096 scans, requiring approximately 16 minutes per spectrum. While this reduces the noise level, it also can lead to some mis-cancellations between the background and sample spectra leading to artefacts. The peaks that are labelled in Fig. 2 are reproducible, while other features, such as the peaks at about 3400 cm^{-1} in the 200 K spectrum and 1500 cm^{-1} in the 250 K spectrum, are not.

The most significant changes occur in the lower wavenumber range and Fig. 3 shows spectra from 1150 to 1750 cm^{-1}, which were obtained with 1024 scans, which eliminates some of the artefacts seen with 4096 scans in Fig. 2. As before, the 150 K anneal causes the 1646 cm^{-1} peak to disappear and be replaced by peaks at 1562 and 1359 cm^{-1}. The 1359 cm^{-1} peak is accompanied by a weak feature at about 1390 cm^{-1} in the 150 K spectrum, and this region shows some possible structure in the 200 K spectrum, which may be indicative of incomplete conversion of HCN to CNH_2. The spectra show little change from 200 to 350 K, demonstrating the stability of CNH_2 on the Pd(111) surface.

The assignment of the CNH_2 peaks seen in Fig. 3 is aided by repeating the experiment with $H^{13}C^{14}N$ and $H^{12}C^{15}N$ and spectra with these isotopologues analogous to those of Fig. 3 are given in the ESI.† Fig. 4 shows a comparison of the spectra obtained starting with $H^{12}C^{14}N$, $H^{13}C^{14}N$ and $H^{12}C^{15}N$. Table 2 lists the wavenumber values for the ν(CN) and $\delta(NH_2)$ modes for CNH_2 on Pd(111) along with the corresponding values for CNH_2 on Pt(111). The fact that the peak at 1564 cm^{-1} shifts to 1554 upon ^{15}N substitution but to only 1562 cm^{-1} with

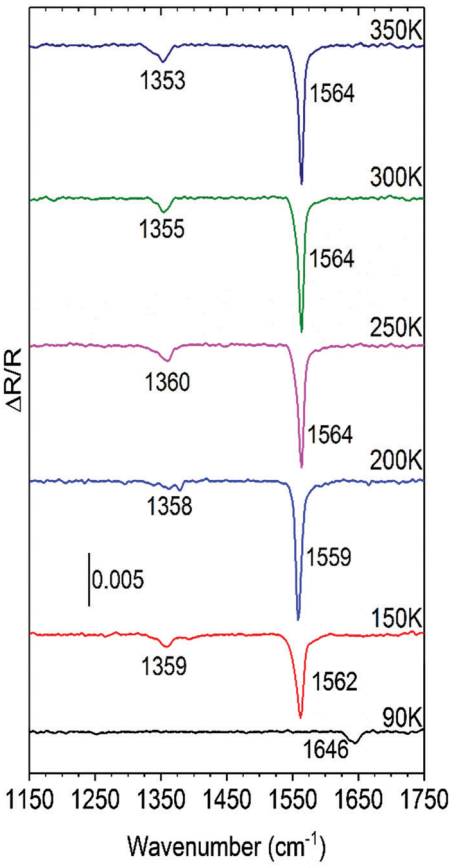

Fig. 3 RAIR spectra of 1.0 L $H^{12}C^{14}N$ on Pd(111) taken at 90 K after annealing for one minute at the indicated temperatures.

^{13}C substitution clearly reveals that this is a $\delta(NH_2)$ mode, rather than a C═N stretch. The large shift of the peak at 1354 to 1342 cm^{-1} with ^{15}N substitution and to 1328 cm^{-1} with ^{13}C substitution clearly indicates that it is a CN stretch mode. The similar positions and isotopic shifts of the peaks on Pd(111) and Pt(111) indicates that the same species, aminocarbyne (CNH_2), forms on both surfaces.

4.2 Computational results

4.2.1 Adsorption of surface intermediates. To help elucidate the mechanism of the decomposition of HCN on Pd(111), we first modelled and calculated various possible intermediates based on prior work on this and similar systems by us and other groups. Table 3 lists and compares their adsorption energies (ΔE_{ads}) calculated using the RPBE and optB86b functionals. Fig. 5 shows the optimized molecular structures of these species. Molecular images in this figure and those below were created using VESTA.[38]

The preferred adsorption sites of several of the species, including di-σ HCN, CN, and atomic H, are consistent with those previously reported by Herron *et al.*[39] CN, CNH, and CNH_2 all preferentially adsorb in upright geometries on the threefold fcc site. We have not found any stable geometry for CN adsorbed on Pd(111) in which the C–N bond is parallel to the surface, in agreement with Herron *et al.* and contradicting Kordesch *et al.*[1]

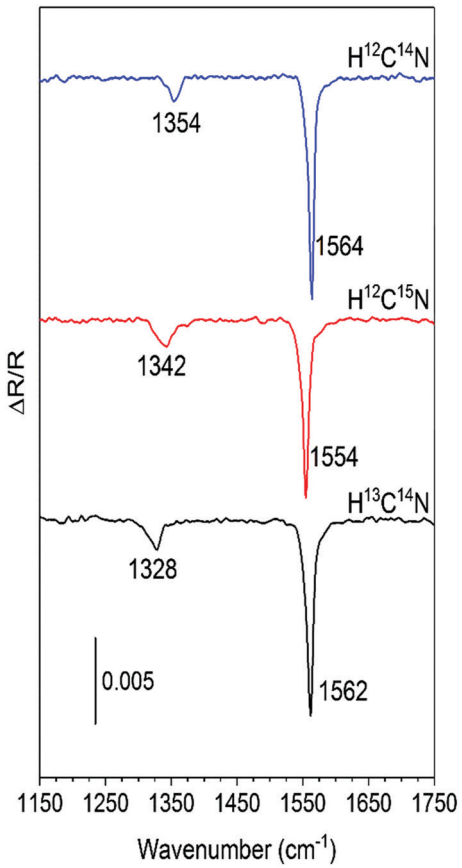

Fig. 4 A comparison of RAIR spectra on Pd(111) taken at 90 K for each isotope after annealing at 300 K for one minute.

Table 2 Peak positions for the ν(CN) and $\delta(NH_2)$ modes of CNH_2 on Pd(111) (experimental and calculated) and Pt(111) (experimental) and ratios, in parentheses, of the positions relative to those of $^{12}C^{14}NH_2$

Mode, isotopologue	Pd(111) (exp.)	Pd(111) (calc.)	Pt(111) (exp.)
ν(CN), $^{12}C^{14}NH_2$	1354	1347	1323
ν(CN), $^{13}C^{14}NH_2$	1328 (0.9808)	1317 (0.9777)	1290 (0.9751)
ν(CN), $^{12}C^{15}NH_2$	1342 (0.9911)	1337 (0.9926)	1312 (0.9917)
$\delta(NH_2)$, $^{12}C^{14}NH_2$	1564	1524	1567
$\delta(NH_2)$, $^{13}C^{14}NH_2$	1562 (0.9987)	1521 (0.9980)	1566 (0.9994)
$\delta(NH_2)$, $^{12}C^{15}NH_2$	1554 (0.9936)	1514 (0.9934)	1559 (0.9949)

Bader analysis indicates that the C atom in CN carries a charge of +0.56 *e* whereas the N atom carries −0.93 *e*, making the CN group overall negatively charged.[40] *cis*- and *trans*-HCNH are included as possible intermediates to CNH_2. The *cis* isomer binds through both C and N in the bridge–top geometry, whereas the *trans* isomer binds through C on the top site only. Atomic N and H prefer to adsorb on the fcc site, whereas atomic C prefers to adsorb on the threefold hcp site. The RPBE adsorption energies of CN, N, and C are noticeably more negative than those reported by Herron *et al.*, which were calculated self-consistently in PW91 and non-self-consistently in RPBE. Non-self-consistent calculations may be insufficient for describing the strong chemical bonding between the C or N and Pd.

Table 3 DFT-calculated minimum-energy adsorption sites and associated adsorption energies (ΔE_{ads}, in eV) of various molecular and atomic intermediates in HCN decomposition on Pd(111), in comparison with available DFT and experimental literature values

Species	Preferred site	ΔE_{ads} GGA-RPBE	ΔE_{ads} optB86b-vdW	DFT lit.[a]	Exp. lit.
HCN upright	top	0.00	−0.56		−0.39[b]
HCN di-σ	top–top|br–br	−0.47	−1.29	−0.42	
$(HCN)_2^{\alpha}$	top–top–br	−0.15[c]	−1.02[c]		
HCNH *trans*	top	−1.75	−2.49		
HCNH *cis*	br–top	−2.21	−3.21		
CNH	fcc	−1.69	−2.40		
CNH_2	fcc	−3.57	−4.48		
CN	fcc	−3.33	−4.08	−3.25	
$(CN)_2$	top–top	−3.11[c]	−3.78[c]		
C	hcp	−6.40	−6.99	−5.80	
N	fcc	−4.29	−5.03	−3.55	
H	fcc	−2.69	−3.06	−2.69	−2.80[d]

Each adsorbate is located on a (2 × 2) surface unit cell at 1/4 ML coverage. ΔE_{ads} is with respect to each adsorbate in gas phase and is non-ZPE corrected. "br" stands for bridge site. [a] From ref. 39. [b] From ref. 42. [c] Per unit of HCN or CN. [d] From ref. 43.

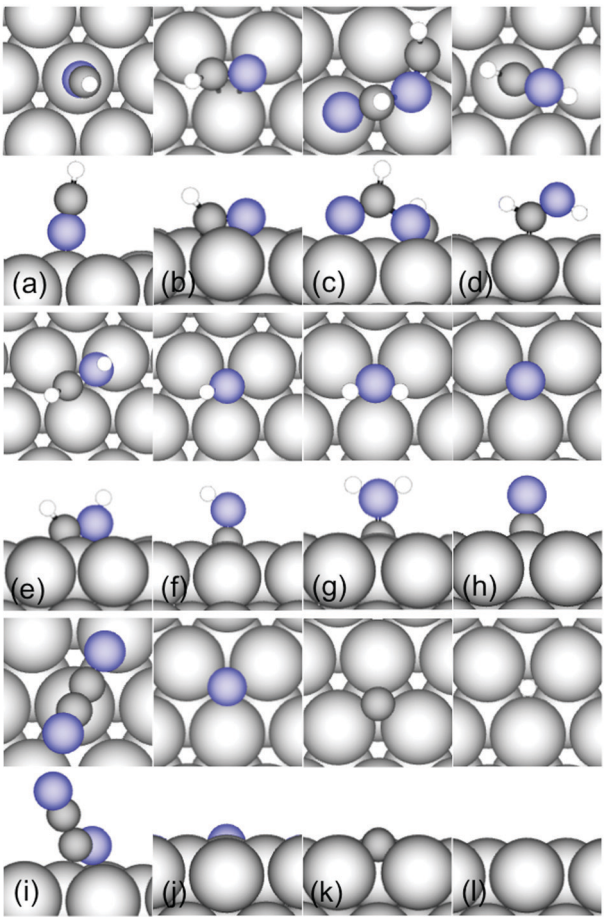

Fig. 5 DFT (optB86b-vdW) calculated minimum-energy adsorption configurations for (a) upright HCN; (b) di-σ HCN; (c) $(HCN)_2$; (d) *trans*-HCNH; (e) *cis*-HCNH; (f) CNH; (g) CNH_2; (h) CN; (i) $(CN)_2$; (j) N; (k) C; (l) H. In each panel, the top view is shown on top and the side view is shown on bottom. Silver, blue, black, and white spheres represent Pd, N, C, and H atoms, respectively. Periodic images of the adsorbates have been removed for clarity.

The fact that the molecular adsorption of upright HCN is not exothermic according to RPBE appears to be inconsistent with its facile reactivity on this surface. A recent study by Hensley *et al.*[41] finds that the contribution of vdW energies to adsorption on transition metal surfaces becomes significant when the values of RPBE ΔE_{ads} fall roughly below 70% of the corresponding ones for optB86b.[41] Based on the adaptive sum method introduced by Hensley *et al.*, we conclude that the optB86b values more closely reflect the actual heats of adsorption for most of the intermediates on Pd(111) (see Table S1, ESI†), although over-binding to some extent by optB86b is expected.

Thus the low-temperature HCN desorption features observed by Guo *et al.*,[42] from which they deduced a maximum desorption barrier of 9.1 kcal mol^{-1} (the α_3 state), most likely corresponded to desorption from the upright HCN state present in a saturated HCN adlayer because the value is consistent with the optB86b ΔE_{ads} of −0.56 eV (−13 kcal mol^{-1}) for upright HCN. The subsequent investigation of the decomposition pathway is conducted based on the optB86b results.

4.2.2 Simulated infrared spectra of intermediates. The IR spectra for various H_xCN intermediates have been simulated and compiled in Fig. 6, which include only the fundamental modes but not overtones. The most prominent features include the $\delta(NH_2)$ mode of CNH_2 (1538 cm^{-1}) and the ν(CH) mode of upright HCN (3366 cm^{-1}). They are in line with the assignment of 1564 cm^{-1} to CNH_2 and 3301 cm^{-1} to HCN. Di-σ HCN is expected to be essentially undetectable with RAIRS due to the lack of any strong mode. CNH, and *cis*- and *trans*-HCNH have several modes with moderate IR intensities. The ν(CN) mode of adsorbed CN is calculated to have a very weak intensity and a frequency of 1922 cm^{-1}, in agreement with the HREELS assignment of 1910 cm^{-1} by Kordesch *et al.* to CN.[1]

We have also simulated IR spectra for isotopically labelled CNH_2 coadsorbed with CN (Fig. 7), for reasons that will be discussed below. The two modes visible in Fig. 7 are the $\delta(NH_2)$ and ν(CN) of CNH_2. As can be seen, the isotopic shifts seen in Fig. 4 are closely captured by the computational results in Fig. 7,

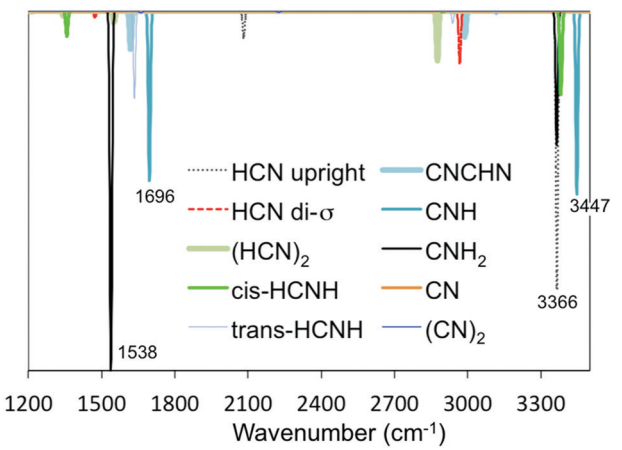

Fig. 6 DFT (optB86b-vdW) calculated IR spectra of possible molecular intermediates formed upon adsorption of HCN on Pd(111). All intermediates calculated at 1/4 ML coverage without any co-adsorbate.

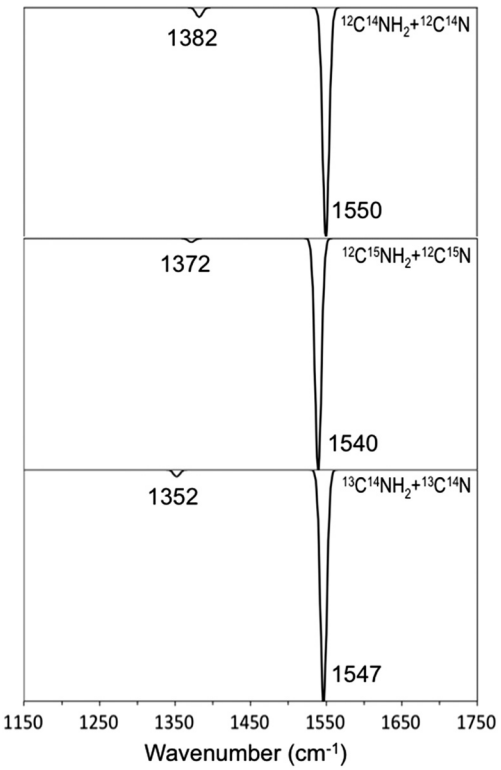

Fig. 7 DFT (optB86b-vdW) calculated IR spectra of normal and isotopically labelled CNH_2 on Pd(111). CNH_2 (in fcc site) is coadsorbed with CN (in hcp site), for an overall coverage of 1/2 ML.

which further confirms the assignment of 1564 cm^{-1} and 1354 cm^{-1} (Fig. 4) to CNH_2.

4.2.3 Reaction pathways for HCN decomposition on Pd(111). We have explored a number of possible reaction pathways to explain the reactivity of HCN following its deposition on Pd(111), including the nature of the hydrogenation/dehydrogenation steps that are operative at cryogenic temperatures. Two minimum-energy reaction pathways are reported below, one uni-molecular (Fig. 8) and the other bi-molecular (Fig. 9). The minimum-energy uni-molecular mechanism for the formation of CNH_2 consists of the steps listed in Table 4, corresponding to what is depicted in Fig. 8.

The upright HCN state, which vibrational analysis indicates to be unstable according to RPBE but which does represent a shallow minimum on the potential energy surface according to optB86b, is predicted to convert to the di-σ state with an essentially zero barrier as an isolated molecule (Fig. 8 and Table 4). This suggests that the upright state cannot exist on the surface except under locally high coverage conditions where its isomerization is sterically hindered.

The minimum energy uni-molecular mechanism does not proceed through HCNH as an intermediate, unlike what was previously proposed by Gómez-Díaz and López for CNH_2 formation on Pt(111).[15] Similar to the energetics that they reported, the uni-molecular hydrogenation/dehydrogenation steps have significant kinetic barriers. Even with ZPE corrections included, the size of the activation energies for the last 3 steps is clearly

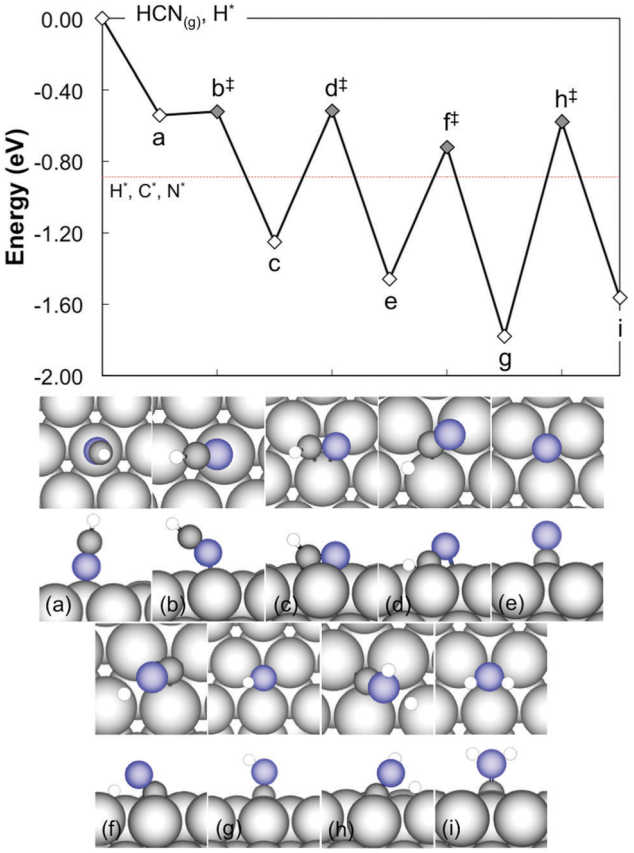

Fig. 8 (upper) DFT (optzB86b-vdw) calculated reaction energy profile for uni-molecular HCN decomposition on Pd(111) at 1/4 ML coverage. (a) Upright HCN, (b) isomerization TS; (c) di-σ HCN; (d) dehydrogenation TS; (e) CN; (f) hydrogenation TS; (g) CNH; (h) hydrogenation TS; (i) CNH_2. "‡" indicates a transition state (TS). Zero on the *y*-axis corresponds to a gas phase HCN molecule and an H atom adsorbed on surface. Horizontal line corresponds to atomic H, C, and N (*i.e.* atomized HCN) at infinite separation from one another. Energies are ZPE-corrected DFT total energies. For brevity, balance of H atoms (at infinite separation) is not indicated. (lower) Snapshots of the surface intermediates and transition states, with top views on top and side views on bottom. Labels correspond to those in the upper panel. Silver, blue, black, and white spheres represent Pd, N, C, and H atoms, respectively.

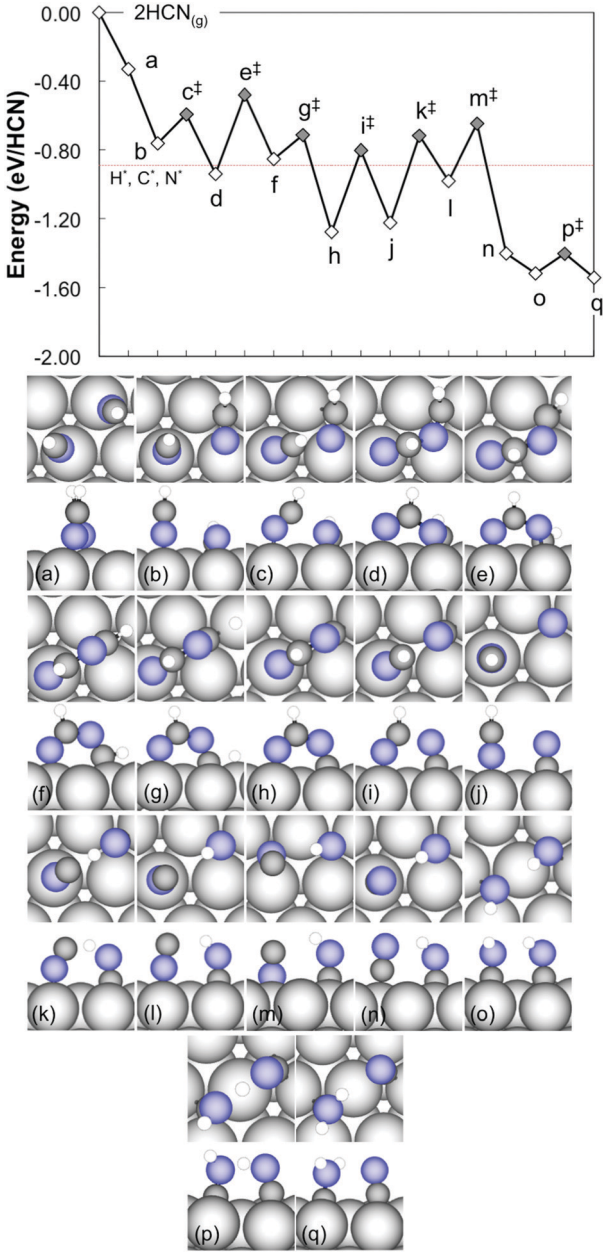

Fig. 9 (upper) DFT (optzB86b-vdw) calculated reaction energy profile for bi-molecular HCN decomposition on Pd(111) at combined 1/2 ML coverage. (a) 2 upright HCN, (b) 1 upright HCN and 1 di-σ HCN; (c) dimerization TS; (d) $(HCN)_2^{\alpha}$; (e) isomerization TS; (f) $(HCN)_2^{\beta}$; (g) dehydrogenation TS; (h) CNCHN; (i) C–N scission TS; (j) HCN and CN; (k) H transfer TS; (l) NC and CNH; (m) flipping TS; (n) CN and CNH; (o) 2 CNH; (p) H transfer TS; (q) CNH_2 and CN. "‡" indicates a transition state (TS). Zero on the *y*-axis corresponds to a gas phase HCN molecule and an H atom adsorbed on surface. Horizontal line corresponds to indicated surface species at infinite separation from one another. Energies are ZPE-corrected DFT total energies. For brevity, balance of H atoms (at infinite separation) is not indicated. (lower) Snapshots of the surface intermediates and transition states, with top views on top and side views on bottom. Labels correspond to those in the upper panel. Silver, blue, black, and white spheres represent Pd, N, C, and H atoms, respectively.

inconsistent with the observed formation of CNH_2 at a temperature as low as 150 K, which implies a maximum barrier of *ca.* 0.4 eV.

We use the semi-classically corrected harmonic transition state theory (SC-HTST) formulated by Fermann *et al.*[44] to estimate the contribution of quantum tunnelling to the reactivity of the last hydrogenation step, which has the highest barrier of the four steps. The eigenvalue of the imaginary mode is found to be 1032 cm^{-1}, which corresponds to a crossover temperature of 239 K. On the other hand, 1.20 eV corresponds to a peak reaction temperature of 462 K, based on Redhead analysis for a second-order rate process with initial coverage of 1 ML and a heating rate of 2 K s^{-1}. Therefore, we conclude that quantum tunnelling does not play a significant role in promoting the uni-molecular mechanism for CNH_2 formation.

Alternatively, we have explored whether bi-molecular interaction can facilitate the formation of CNH_2, and found it to be possible. The bi-molecular mechanism (Fig. 9), which to our knowledge has not been proposed before for HCN on transition

Table 4 Optb86b-vdW calculated forward activation energies (E_a, in eV), reaction energies (ΔE, in eV)[a] in the minimum energy uni-molecular mechanism

Step	E_a	ΔE	E_a^{ZPE}	ΔE^{ZPE}
1. $HCN^{upright} \rightarrow HCN^{di\text{-}\sigma}$	0.01	−0.73	0.00	−0.71
2. $HCN \rightarrow CN + H$	0.93	−0.07	0.74	−0.21
3. $CN + H \rightarrow CNH$	0.79	−0.44	0.74	−0.32
4. $CNH + H \rightarrow CNH_2$	1.23	+0.03	1.20	+0.21

[a] ΔE calculated with species at infinite separation.

Table 5 OptB86b-vdW calculated forward activation energies (E_a, in eV), reaction energies (ΔE, in eV per unit of HCN)[a] in the minimum energy bi-molecular mechanism

Step	E_a	ΔE	E_a^{ZPE}	ΔE^{ZPE}
1. $2HCN \rightarrow (HCN)_2^{\alpha}$	0.17	−0.23	0.17	−0.18
2. $(HCN)_2^{\alpha} \rightarrow (HCN)_2^{\beta}$	0.53	+0.10	0.46	+0.09
3. $(HCN)_2^{\beta} \rightarrow CNCHN + H$	0.25	−0.38	0.14	−0.43
4. $CNCHN \rightarrow CN + HCN$	0.56	+0.10	0.48	+0.06
5. $CN + HCN \rightarrow CNH + NC$	0.61	+0.25	0.51	+0.24
6. $CNH + NC \rightarrow CNH + CN$	0.35	−0.43	0.34	−0.42
7. $2CNH \rightarrow CNH_2 + CN$[b]	0.20	−0.04	0.11	−0.02

[a] ΔE calculated with organic species co-adsorbed in same (2 × 2) surface unit cell. Balance of H is placed at infinite separation. [b] ΔE calculated with additional CN and H at infinite separation.

metals, consists of the steps listed in Table 5. All steps except one involve two (or two units of) HCN or its derivatives reacting with each other. The pathway begins with an upright HCN coupling *via* its C atom to the N atom of a di-σ HCN, yielding a dimer state ($(HCN)_2^{\alpha}$). This species is reminiscent of the known HCN trimer, *s*-triazine, and its formation is consistent with the tendency of HCN to polymerize due to its possession of both a nucleophilic N and an electrophilic C. This step has a small barrier of 0.17 eV, below the negative of the ΔE_{ads} of the upright HCN state. After structural rearrangement, the dimer state $(HCN)_2^{\beta}$ undergoes dehydrogenation with a low activation energy of 0.14 eV. The remaining fragment, CNCHN, then undergoes an intramolecular CN bond scission to produce a CN group and an upright HCN. An intermolecular H transfer between the two species yields a CNH and an NC group binding through the N atom to a top site. The NC species is significantly less stable than the CN group, and it undergoes rapid conversion to the latter through a flipping movement. Finally, two CNH molecules undergo another intermolecular H transfer to produce CNH_2 and CN. The highest kinetic barrier is 0.51 eV (Step 5), which is much more in line with the observed low-temperature reactivity of HCN. Due to the involvement of upright HCN, a locally high coverage would be required to stabilize the state, which implies that this mechanism would not be operative at very low initial HCN coverages. We have used the approach by Herron *et al.*[39] to estimate the diffusion barriers for upright and di-σ HCN. Both are estimated to be less than 0.1 eV, indicating that surface mobility does not preclude adsorbed HCN molecules from finding and reacting with one another on Pd(111).

The pathway produces coadsorbed CNH_2 and CN, which stabilize each other (by 0.22 eV, with ZPE, same below) and are slightly more stable than a pair of coadsorbed CNH (by 2 × ΔE = −0.04 eV). On an isolated basis, as indicated by the dashed lines in Fig. 9, CNH is more stable than CNH_2 (by 0.11 eV, or 0.18 eV with RPBE). Thus, although DFT predicts CNH_2 to be a stable product, it is not predicted to be overwhelmingly more stable than CNH. This is potentially a significant discrepancy with experiment, which finds no vibrational signature attributable to CNH on Pd(111). Whether this is due to any intrinsic error of DFT requires further investigation.

Table 6 OptB86b-vdW calculated energies (in eV) for several possible states of HCN on Cu(100), Pd(111), and Ru(001)

State	Cu(100)	Pd(111)	Ru(001)
Upright HCN	−0.32	−0.54	−0.91
Di-σ HCN	−0.79	−1.25	−2.05
CN + H	−1.17	−1.46	−2.20
CNH_2	−0.83	−1.57	−1.80
All atoms	+0.04	−0.89	−2.80

Energy is referenced to a clean surface, gas phase HCN, and an adsorbed H atom and is calculated on (2 × 2) surface unit cells. CN prefers a di-σ geometry with the C–N bond axis parallel to the surface on Cu(100) and Ru(001). Multiple species in the same state are calculated at infinite separation.

In any case, this mechanism predicts that following the formation of CNH_2, the surface has a significant amount of CN and atomic H coexisting with CNH_2 since for every CNH_2, 3 CN molecules and 2 H atoms are formed. The presence of excess H atoms on the surface is consistent with the TPD findings of Guo *et al.*,[42] who reported a H_2 desorption peak *ca.* 300 K that resembles the 2nd order desorption of pure hydrogen from Pd(111).[45]

We have also calculated the energy of adsorbed atomic H, C, and N (representing the complete atomization of HCN), which are less stable than di-σ HCN, CN, CNH, and CNH_2 (Fig. 8), indicating that thermodynamics does not favour complete dissociation of HCN on Pd(111), which is indeed not observed experimentally. To shed light on the fate of HCN on Ru(001) and Cu(100), we compare the energies of several possible states, including upright and di-σ HCN, CN + H, CNH_2, and all atoms on Pd(111), Ru(001), and Cu(100) in Table 6. The energies for the species on Pd(111) are those plotted in Fig. 8. On Ru(001) the completely atomized state has by far the lowest energy, at −2.80 eV, which suggests a significant driving force toward atomization on Ru(001) and is consistent with the fact that only upright HCN is observed on Ru(001). On Cu(100) thermodynamics favours CN + H. Whether HCN dissociation is kinetically more facile than HCN desorption will be the subject of a future study. We note that H_2 desorption is known to occur at lower temperature on Cu(100)[46] than on Pd(111). Thus monitoring H_2 desorption in a TPD study of HCN on Cu(100), which has not been performed to our knowledge, would provide definitive evidence whether HCN dissociates on Cu(100).

5. Discussion

The pathway that we have found for CNH_2 formation on Pd(111) from HCN allows new insights into the previously published

studies on this system. The HREELS results are similar to what we observe but the assignments were quite different.[2] For a 0.1 L HCN exposure to Pd(111) at 300 K, loss peaks were observed at 1290 and 1540 cm^{-1}, which given the HREELS resolution of 65 cm^{-1}, are close to our values of 1354 and 1564 cm^{-1}. They also found that the expected peak in the CH/NH stretch region was too weak to observe for low exposures at 300 K. They assigned their 1540 cm^{-1} peak to a C═N stretch and the 1290 cm^{-1} peak to the HCN bend, with the assumption that it was stiffened upon adsorption. In a separate study by the same authors, the HCN bend position was assigned to an HREELS peak at 1355 cm^{-1}.[1] These values are essentially at the same position, within the margin of error, as the peaks that we observe at 1354 and 1564 cm^{-1} and assign to the $\delta(NH_2)$ and $\nu(CN)$ modes of CNH_2. We therefore conclude that the 300 K HREELS data is better assigned to CNH_2 than to a di-σ bonded HCN species. Other earlier observations are also consistent with CNH_2 on Pd(111). For example, it was noted that the same spectra were obtained from HCN adsorption as from the hydrogenation of CN produced from the dissociation of cyanogen.[47] On Pt(111), we showed that CN produced from cyanogen dissociation is readily hydrogenated to CNH_2, and it follows that the same reaction occurs on Pd(111).[48]

The orientation of the CN bond of the proposed di-σ bonded HCN was investigated with NEXAFS and the data indicated that the CN bond was parallel to the surface.[1] For the adsorbed diatomic molecules CO, NO, and CN, the NEXAF spectra at the N 1s edge show a sharp π resonance at the threshold and a broader σ resonance at higher photon energy. The σ/π intensity ratio depends on the angle (θ_E) between the surface normal and the electric field vector and is much larger for CO and NO than it is for CN. As the former are bonded perpendicular to the surface, it was concluded that CN was bonded parallel to the surface. They then argued that because the NEXAFS results for HCN resembled the results for CN, that the CN bond of HCN was also parallel to the surface. This is in contrast to our findings that HCN exposure at room temperature leads to both CN and CNH_2 on the surface Although we do not detect adsorbed CN experimentally, the calculations indicate that it is oriented perpendicular to the surface, as is the CN bond of CNH_2. The calculations imply that di-σ bonded HCN should be a stable intermediate with the CN axis parallel to the surface, but there is no evidence for it from our RAIR spectra. Similar considerations would apply to an angle-resolved ultraviolet photoelectron spectroscopy (ARUPS) study.[49] Spectra obtained after annealing to 200 K an HCN layer adsorbed at 110 K should have produced a mixture of CN and CNH_2. The resulting ARUP spectra display four distinct peaks and their angular dependencies were carefully characterized. However, the discussion indicated that there was some ambiguity in interpreting the results in terms of a di-σ bonded HCN with the CN bond parallel to the surface. While it is difficult to reconcile the results from NEXAFS and ARUPS with our results using RAIRS, it is possible that the former techniques detect species that are invisible to the latter.

Our findings can also provide new insights into a thorough study of the reaction chemistry of HCN on Pd(111) as studied with TPRS by Guo *et al.*[42] Following an HCN exposure of 2.6×10^{15} molecules per cm^2 at a surface temperature of 87 K, three desorption products were observed: HCN, H_2, and C_2N_2. Multilayer HCN was observed to desorb as two peaks (α_1 and α_2) at 118 and 131 K and monolayer HCN as a peak (α_3) at 150 K. A single higher temperature HCN desorption peak (β_1) was observed at 400 K. The latter was accompanied by reaction limited H_2 desorption (β_2). A desorption-limited H_2 peak (β_1) was observed at lower temperatures, with the exact temperature depending on HCN exposure. Cyanogen desorption was observed in the temperature range of 500 to 750 K. No surface carbon or nitrogen was detected with Auger electron spectroscopy after cyanogen desorption, indicating that the CN bond remains intact throughout the reaction pathway. Our limited TPRS results roughly matched those of Guo *et al.*,[42] although we were unable to detect cyanogen desorption, which was almost certainly due to a lower sensitivity in our TPRS experiments compared to theirs.

In contrast to the results obtained following HCN exposures at 87 K, high HCN exposures with the Pd(111) surface at 300 K led to the formation of a $(HCN)_x$ polymeric species.[42] Upon heating, $(HCN)_x$ decomposes to liberate HCN (β_2 HCN) at temperatures as high as 800 K. The amount of β_2 HCN desorbing following 300 K exposures is much greater than observed following low temperature exposures and increases linearly with HCN exposure, indicating that it forms a multilayer polymer. Although we did not explore such a polymeric species in this study, our computational results suggesting a mechanism involving HCN dimers also reflects the tendency of the HCN molecule to form bonds with itself.

Our results can provide new insights into the origin of the β_1 HCN and β_1 and β_2 H_2 peaks observed by Guo *et al.*[42] We can associate the β_1 H_2 peak with the decomposition of the $(HCN)_2^{\beta}$ dimer to produce CNCHN + H, with the H atom stable on the surface until the recombinative H_2 desorption temperature is reached. Guo *et al.*[42] found that for the lowest exposures to the Pd(111) crystal at 300 K, β_2 H_2 occurs at 375 K and β_1 HCN at 510 K. As these peaks are associated with reaction-limited desorption, and from RAIRS we observed the disappearance of CNH_2 for annealing temperatures above 350 K, the simplest conclusion is that β_1 HCN and β_2 H_2 are associated with CNH_2 decomposition. We further assume that CNH_2 decomposes by the reverse of the uni-molecular mechanism (Step 4, Table 4) to produce H, which immediately desorbs as β_2 H_2, and adsorbed CNH. The latter is then assumed to be stable to higher temperatures, but eventually desorbs as β_1 HCN. As the coverage increases, intermolecular interactions change the energetics of various steps such that the β_1 HCN and β_2 H_2 peaks moved closer together as the coverage increased to the point where both molecules desorbed at the same temperature of 400 K.

The experimental evidence for an upright bonding configuration for HCN on Pd(111) at low temperatures is quite clear from the RAIR spectra. When van der Waals contributions are included with the optB86b-vdW functional, an isolated, weakly bound but stable upright HCN is obtained from DFT. However, the upright HCN can be stabilized in the presence of a neighbouring di-σ

bonded HCN (Fig. 9). This is only consistent with the experimental RAIRS results if we assume that the peaks of di-σ bonded HCN are too weak to observe. The calculated spectra imply that this would be the case. Similarly, although the experimentally implied pathway involves adsorbed CN, DFT indicates that it would likely be undetectable with RAIRS. The calculations predict two strong RAIRS peaks for the CNH intermediate, but these peaks are not observed in the experiments for HCN on Pd(111). However, on Pt(111), a peak was observed at 3348 cm^{-1}, the intensity of which rose and fell as HCN was converted to CNH_2, and was therefore attributed to the NH stretch CNH. This peak was not accompanied by an observable CN stretch, in contrast to the DFT prediction in Fig. 6. Also, the position of the experimental 3348 cm^{-1} peak fell between that of the CH stretch of adsorbed HCN and the NH stretch of CNH_2, whereas DFT implies that the NH stretch of CNH would lie above the NH stretch of CNH_2. Coincidently, the NH stretch of CNH_2 is calculated to be at the same value as the CH stretch of upright HCN, which is not observed in the experimental spectra. The calculations predict moderately intense peaks for both *cis*- and *trans*-HCNH, but no peaks assignable to these species are observed with RAIRS, implying that HCNH is not a stable intermediate.

6. Conclusions

The initial adsorption of HCN on Cu(100), Pt(111), Pd(111), and Ru(001) at temperatures below 100 K is characterized by a relatively sharp CH stretch at about 3300 cm^{-1}. This value is close to that of the gas phase and is characteristic of a CN triple bond. This implies that this peak corresponds to an HCN molecule that does not bond in a way that involves rehybridization of the carbon atom. The overall spectral characteristics indicate that this form of HCN bonds to these surfaces through the nitrogen lone pair and is oriented with the molecular axis perpendicular to the surface. The DFT calculations imply that an upright HCN would be stabilized through interaction with a neighbouring HCN molecule bonded with the CN axis parallel to the surface. Both the experimental and calculated RAIR spectra, including isotopic shifts, demonstrate that CNH_2 forms on Pd(111). The RAIR spectra of CNH_2 on Pd(111) are almost identical to the spectra on Pt(111). The DFT calculations indicate that a bi-molecular mechanism for formation of CNH_2 from HCN with low barriers is available that can explain the observation of CNH_2 at relatively low temperatures. However, the bi-molecular mechanism involves intermediates that are not detected with RAIRS.

Conflicts of interest

There are no conflicts to declare.

Acknowledgements

We thank Ravi Ranjan, Hamzzat Soyege, and Jonathon Kruppe for assistance with the experiments. The experimental work was supported by a grant from the National Science Foundation, CHE-1800236. The computational work was supported by the Donors of the American Chemical Society Petroleum Research Fund. High performance computational resources were provided by the Louisiana Optical Network Infrastructure (http://www.loni.org) and by the National Energy Research Scientific Computing Center, which is supported by the Office of Science of the U.S. Department of Energy under contract #DE-AC02-05CH11231.

References

1 M. E. Kordesch, T. Lindner, J. Somers, W. Stenzel, H. Conrad, A. M. Bradshaw and G. P. Williams, *Spectrochim. Acta, Part A*, 1987, **43**, 1561–1566.
2 M. E. Kordesch, W. Stenzel and H. Conrad, *Surf. Sci.*, 1988, **205**, 100–116.
3 D. Jentz, H. Celio, P. Mills and M. Trenary, *Surf. Sci.*, 1995, **341**, 1–8.
4 D. Jentz, P. Mills, H. Celio, M. Belyansky and M. Trenary, *J. Chem. Phys.*, 1996, **105**, 3250–3257.
5 D. Jentz, P. Mills, H. Celio and M. Trenary, *Surf. Sci.*, 1996, **368**, 354–360.
6 H. Celio, P. Mills, D. Jentz, Y. I. Pae and M. Trenary, *Langmuir*, 1998, **14**, 1379–1383.
7 X. Hu and M. Trenary, *J. Phys. Chem. C*, 2012, **116**, 4091–4096.
8 X. Hu, J. Yin, R. J. Meyer and M. Trenary, *J. Phys. Chem. C*, 2015, **119**, 14506–14512.
9 G. E. Hyde and D. F. Hornig, *J. Chem. Phys.*, 1952, **20**, 647–652.
10 T. Nakagawa and Y. Morino, *Bull. Chem. Soc. Jpn.*, 1969, **42**, 2212–2219.
11 J. Pacansky and G. V. Calder, *J. Mol. Struct.*, 1972, **14**, 363–383.
12 R. B. Bohn and L. Andrews, *J. Phys. Chem.*, 1989, **93**, 3974–3979.
13 B. Chatterjee, D. H. Kang, E. Herceg and M. Trenary, *J. Chem. Phys.*, 2003, **119**, 10930–10940.
14 D. C. Ford, Y. Xu and M. Mavrikakis, *Surf. Sci.*, 2005, **587**, 159–174.
15 J. Gómez-Díaz and N. López, *J. Phys. Chem. C*, 2011, **115**, 5667–5674.
16 C. W. J. Bol, J. D. Kovacs, M. Chen and C. M. Friend, *J. Phys. Chem. B*, 1997, **101**, 6436–6442.
17 A. Kis, R. Barthos and J. Kiss, *Phys. Chem. Chem. Phys.*, 2000, **2**, 4237–4241.
18 X. Feng, M. K. Abdel-Rahman, C. M. Kruppe and M. Trenary, *Surf. Sci.*, 2017, **664**, 1–7.
19 I. Waluyo, Y. Ren and M. Trenary, *J. Phys. Chem. Lett.*, 2013, **4**, 3779–3786.
20 P. L. Hagans, I. Chorkendorff and J. T. Yates, *J. Phys. Chem.*, 1988, **92**, 471–476.
21 G. Kresse and J. Furthmüller, *Phys. Rev. B: Condens. Matter Mater. Phys.*, 1996, **54**, 11169.
22 J. Klimeš, D. R. Bowler and A. Michaelides, *J. Phys.: Condens. Matter*, 2010, **22**, 022201.

23 J. Klimeš, D. R. Bowler and A. Michaelides, *Phys. Rev. B: Condens. Matter Mater. Phys.*, 2011, **83**, 195131.
24 B. Hammer, L. B. Hansen and J. K. Nørskov, *Phys. Rev. B: Condens. Matter Mater. Phys.*, 1999, **59**, 7413–7421.
25 P. E. Blöchl, *Phys. Rev. B: Condens. Matter Mater. Phys.*, 1994, **50**, 17953–17979.
26 G. Kresse and D. Joubert, *Phys. Rev. B: Condens. Matter Mater. Phys.*, 1999, **59**, 1758.
27 M. Methfessel and A. T. Paxton, *Phys. Rev. B: Condens. Matter Mater. Phys.*, 1989, **40**, 3616–3621.
28 N. W. Ashcroft and N. D. Mermin, *Solid State Physics*, Holt, Rinehart and Winston, New York, 1976.
29 J. Neugebauer and M. Scheffler, *Phys. Rev. B: Condens. Matter Mater. Phys.*, 1992, **46**, 16067–16080.
30 G. Henkelman, B. P. Uberuaga and H. Jónsson, *J. Chem. Phys.*, 2000, **113**, 9901–9904.
31 G. Henkelman and H. Jónsson, *J. Chem. Phys.*, 1999, **111**, 7010–7022.
32 S. R. Bahn and K. W. Jacobsen, *Comput. Sci. Eng.*, 2002, **4**, 56–66.
33 R. E. Hoffman and D. F. Hornig, *J. Chem. Phys.*, 1949, **17**, 1163.
34 H. B. Friedrich and P. F. Krause, *J. Chem. Phys.*, 1973, **59**, 4942–4948.
35 P. A. Gerakines, M. H. Moore and R. L. Hudson, *Icarus*, 2004, **170**, 202–213.
36 I. Couturier-Tamburelli, N. Pietri, V. Le Letty, T. Chiavassa and M. Gudipati, *Astrophys. J.*, 2018, **852**, 117.
37 K. N. Choi and E. F. Barker, *Phys. Rev.*, 1932, **42**, 777–785.
38 K. Momma and F. Izumi, *J. Appl. Crystallogr.*, 2008, **41**, 653–658.
39 J. A. Herron, S. Tonelli and M. Mavrikakis, *Surf. Sci.*, 2012, **606**, 1670–1679.
40 M. E. Kordesch, W. Stenzel and H. Conrad, *Surf. Sci.*, 1987, **186**, 601–623.
41 A. J. R. Hensley, K. Ghale, C. Rieg, T. Dang, E. Anderst, F. Studt, C. T. Campbell, J.-S. McEwen and Y. Xu, *J. Phys. Chem. C*, 2017, **121**, 4937–4945.
42 X. Guo, A. Hoffman and J. T. Yates, *J. Phys. Chem.*, 1989, **93**, 4253–4258.
43 J. Wellendorff, T. L. Silbaugh, D. Garcia-Pintos, J. K. Nørskov, T. Bligaard, F. Studt and C. T. Campbell, *Surf. Sci.*, 2015, **640**, 36–44.
44 J. T. Fermann and S. Auerbach, *J. Chem. Phys.*, 2000, **112**, 6787–6794.
45 G. E. Gdowski, T. E. Felter and R. H. Stulen, *Surf. Sci.*, 1987, **181**, L147–L155.
46 P. B. Rasmussen, P. M. Holmblad, H. Christoffersen, P. A. Taylor and I. Chorkendorff, *Surf. Sci.*, 1993, **287–288**, 79–83.
47 M. E. Kordesch, W. Stenzel and H. Conrad, *Surf. Sci.*, 1986, **175**, L687–L692.
48 P. Mills, D. Jentz and M. Trenary, *J. Am. Chem. Soc.*, 1997, **119**, 9002–9009.
49 J. S. Somers, M. E. Kordesch, R. Hemmen, T. Lindner, H. Conrad and A. M. Bradshaw, *Surf. Sci.*, 1988, **198**, 400–412.

